

# Quasiparticles in Iron Silicides: GW versus LDA

Natalia Zamkova,<sup>1,2</sup> Vyacheslav Zhandun,<sup>1</sup> Sergey Ovchinnikov,<sup>1,2</sup> and Igor Sandalov<sup>1,3,\*</sup>

<sup>1</sup>*L.V.Kirensky Institute of physics, Siberian Branch of Russian Academy Sciences, 660036 Krasnoyarsk, Russia*

<sup>2</sup>*Siberian Federal University, 660041 Krasnoyarsk, Russia*

<sup>3</sup>*Applied Materials Physics, Department of Materials Science and Engineering,  
KTH Royal Institute of Technology, SE 100 44 Stockholm, Sweden*

The angle-resolved photoemission spectroscopy (ARPES) is able to measure both the spectra and spectral weights of the quasiparticles in solids. Although it is common to interpret the band structure obtained within the density-functional-theory based methods as quasiparticle spectra, these methods are not able to provide the changes in spectral weights of the electron excitations. We use Vienna Ab initio Simulation Package (VASP) for evaluation of the quasiparticle spectra and their spectral weights within Hedin's GW approximation (GWA) for  $Fe_3Si$  and  $\alpha-FeSi_2$ , providing, thus, a prediction for the ARPES experiments. Comparison of the GGA-to-DFT and GWA band structures shows that both theories reflect peculiarities of the crystal structures in similar shape of the bands in certain  $k$ -directions, however, in general the difference is quite noticeable. We find that the GWA spectral weight of quasiparticles in these compounds deviates from unity everywhere and shows non-monotonic behavior in those parts of bands where the delocalized states contribute to their formation. Both methods lead to the same conclusion: those of iron ions in  $Fe_3Si$  which occupy the positions  $Fe^{(1)}$ , where they are surrounded by only  $Fe$  ions ( $Fe^{(2)}$  positions), have the  $d$ -electrons localized and large magnetic moment whereas  $Fe$  ions in the  $Fe^{(2)}$  positions with the  $Si$  nearest neighbors have  $d$ -electrons delocalized and the magnetic moments quenched. The  $Si$  influence on the  $Fe$  ion state is even more pronounced in the  $\alpha-FeSi_2$  where all iron ions have the  $Si$  ions as nearest neighbors: both GWA and GGA calculations produce zero moment on iron ions.

The advantages and disadvantages of both approaches are discussed.

PACS numbers: 71.20.Be, 71.20.Eh, 71.20.Gj, 75.20.Hr, 75.47.Np,  
71.20.-b, 75.10.Lp, 71.15.Dx, 71.70.Ch, 71.45.Gm

## I. INTRODUCTION

A hope to use the electron spin additionally to the charge as an information carrier has led to a development of the spintronics. One feasible way to exploit the spin degrees of freedom is to synthesize such magnetic semiconductors, which, on the one hand, should be magnetic at room temperature, and, on the another hand, should be easily integrated with existing semiconductor industry. Therefore, it is desirable that it should be  $Si$  based<sup>1</sup>. A magnetic moment can be added by a transition-metal constituents. The other way is to use a magnetic metal for injecting of spin-polarized electrons into, say,  $Si$ -based semiconductor. The technologies which create magnetic epitaxial multi-layer films on  $Si$ , produce an interface, which contains the compounds of  $TSi$ , where  $T$  is a transition metal. This makes iron silicides compounds highly perspective materials both in bulk and film form and a detailed understanding of their physics is on demand. Recently the formation of single crystalline  $Fe_3Si$  phases in the  $Fe/Si$  interface has been demonstrated by several groups<sup>2-4</sup>. The theoretical understanding of the ground-state properties like cohesive and structural properties is achieved long ago via first-principle calculations based on the various realization of local-density approximation to density functional theory<sup>5-10</sup>.

However, the experiments, that measure differential

information (not thermodynamics), require for their interpretation a knowledge of the single-particle-*excitation* properties. For example, all photoeffect-based measurements belong to this class. The photoemission spectroscopy (**PES**) provides direct measurement of the energy of electronic quasiparticles. Its extension, the angle-resolved PES (**ARPES**), which uses the synchrotron radiation facilities, allows for extracting also perpendicular to surface momentum dependence of quasiparticle energy. Further refinement, the laser-based ARPES provides even better accuracy and resolution. Recently developed method, the time-resolved two-photon photoemission (**TR-2PPE**) spectroscopy<sup>11</sup>, can monitor the state of an excited electron during the course of its transformation by laser-induced surface reaction. Probably, this is the only method capable to directly measure the quasi-particle's life-time. The transport and tunneling experiments are even more evident examples where the quasiparticle concept is a necessary ingredient for understanding the underlying physics. However, general theories sometimes are not sufficient for describing real materials. For example, the predictions of the life-times within the Landau theory of Fermi-liquid do not describe the experiments even on  $Al$  and noble metals<sup>12</sup>, contrary to the expectation. Indeed, electrons in these metals are well delocalized and expected to behave as a good Fermi-liquid. Furthermore, TR-2PPE experiments show that the lifetime of an excited electron in  $Al$  at a fixed energy  $E < E_F$  depends on the frequency of the pump pulse, i.e.,

on the band from which the electron originated. These examples convince that *ab initio* calculations for real materials are required. The most developed method of electronic structure calculations, which is based on density functional theory, is designed and applicable for the ground state properties only<sup>12, 19</sup>. This gives rise to certain doubts that the electronic bands obtained within the framework density functional theory (DFT) by means of local-(spin)-density approximation with or without gradient corrections, can be interpreted as energies of excited states. Nevertheless, the band structure, generated by Kohn-Sham equations, is ubiquitously exploited as quasiparticle spectrum. Here we will compare the results of calculations within the version of gradient-corrected local-density approximation to density functional theory (GGA) and GW approximation (GWA)<sup>12</sup>. In the latter  $G$  is the Green's function and  $W$  is the screened Coulomb interaction. Both approaches have their own advantages and disadvantages. The exchange-correlation potential used in all modern implementations of the Kohn-Sham machinery contains the correlation effects that are much beyond the random phase approximation used in GWA. Nevertheless the DFT based approach has the essential drawbacks that i) the exchange-correlation potential is calculated for the homogeneous electron gas, and the transfer of these results to the inhomogeneous electron gas of real materials is not easy to justify, and ii) it is difficult to improve the calculations by adding in a controlled way some corrections. The convincing example of it is the widely used LDA+U approximation, where many different forms of double-counting corrections are in use: the way to make it in a controlled way is not found yet. The GW method does not contain this problem, it is well controlled approximation. The strong advantage of GWA is that it results in real quasiparticle excitations. However, it requires much more of computer resources than, say, GGA. It is expected that they should produce approximately the same band structure, since both approaches ignore the intraatomic (often strong) correlations. If the problem of interest does not require the knowledge of the spectral weights and/or is intended to use it as a first step for a better approximations, it is preferable to use GGA. The latter usually is used as a perturbational input for GWA. For this reason it makes sense to compare both quasiparticle and Kohn-Sham band structures and to analyse the difference between the exchange-correlation potential and the real part of the GW self energy. Since the eigenvalues of the Kohn-Sham (KS) equations cannot be interpreted as quasi-particle (QP) excitations whereas the band structure generated by the GW method can, we calculate GW QP energies. They can serve as a prediction of ARPES measurements on iron silicides.

The paper is organized as follows. In Sec. II we present the details of our *ab initio* DFT and GW calculations and give brief discussion of their advantages and drawbacks. The comparison of band structure and density

of electron states calculations of iron silicides  $Fe_3Si$  and  $\alpha - FeSi_2$  obtained by both methods is given in Sec. III and in Sec. IV we discuss results and make conclusions.

## II. THE METHODS: GW VERSUS GGA FOR IRON SILICIDES

### A. Band structure and excitation energies.

The question if the DFT band structure can be interpreted as single-electron excitations' energies have been discussed repeatedly (see, *e.g.*,<sup>5</sup>, review<sup>18</sup> and the book<sup>19</sup>). The single-electron Green's function by definition describes the transitions between  $n$  and  $(n \pm 1)$  electron states, and the solutions of the Dyson's equation provide the excitation energies and their spectral weights. The potential in the Kohn-Sham equation does not depend on energy and automatically loses information on possible deviations of the spectral weight of quasi-particles from unity. Although the DFT based methods have been designed for the investigation of the ground-state properties and, it seems, there are no grounds for interpreting the band structure, generated by the Kohn-Sham equations as the energies of the single-electron excitations. However, the question about such a possibility is not so trivial and cannot be ruled out by this argument only. First, one can notice that the same statement holds for the Hartree-Fock-determinant wave function of the *ground state*, for which Koopmans<sup>20</sup> proved that in closed-shell Hartree - Fock theory, the first ionization energy of a molecular system is equal to the negative of the orbital energy of the highest occupied molecular orbital. There is an analogue of the Koopmans' theorem for DFT<sup>21</sup>. Second, Hohenberg-and-Kohn's proof<sup>22</sup> that the total energy of a system with interaction is a unique functional of the electron density  $\rho(\mathbf{r})$  led Sham and Schlueter<sup>23</sup> to the equation, which, at least, in principle, allows calculation of the exchange-correlation potential in DFT for any chosen approximation for the electron-Green's-function self-energy  $\Sigma'$ . Schematically,  $G^{-1} = (G_0^{-1} - v_{xc}) + v_{xc} - \Sigma'$  gives  $G = G_{DFT} + G_{DFT} (v_{xc} - \Sigma') G$ . Here  $G_0$  is the Green's function of electrons in the Coulomb field of nuclei and Hartree potential and the prime in  $\Sigma'$  means that the Hartree term is subtracted,  $\Sigma' = \Sigma - v_{Hartree}$ . Expressing then the charge densities in terms of  $G$ ,  $\rho = \langle G \rangle_E$ , i.e., taking appropriate contour integral over energy from both sides and using the equality  $\rho_{model}^{DFT}(r) = \rho_{genuine}(r)$  one finds  $0 = \langle G_{DFT} (v_{xc} - \Sigma') G \rangle_E$ . This equation<sup>23</sup> establishes the correspondence between the self-energy and the exchange-correlation potential. For this reason one can hope that at least for the  $v_{xc}$  found for certain  $\Sigma'$  the self-energy-based and Kohn-Sham eigenvalues coincide. The problem is, however, that the eigenvalues  $\varepsilon_{kn}$  and wave functions  $\varphi_{kn}(r)$  of Kohn-Sham equation,

$$\left[ \frac{p^2}{2m} + v_{e-n}(r) + v_{Hartree}(r) + v_{xc}(r) \right] \varphi_{kn}(r) = \varepsilon_{kn} \varphi_{kn}(r), \quad (1)$$

and its self-energy-based counterpart,

$$\left[ \frac{p^2}{2m} + v_{e-n}(r) + v_{Hartree}(r) \right] \Phi_{kn}(r, E_{kn}) + \int dr_1 Re\Sigma'(r, r_1, E_{kn}) \Phi_{kn}(r_1, E_{kn}) = E_{kn} \Phi_{kn}(r, E_{kn}), \quad (2)$$

represent more differential information than the electron densities and, to the best of our knowledge, a prove of a statement that  $\varepsilon_{kn} = E_{kn}$  does not exists ( here  $n$  labels the bands). To be more precise, Eq.(2) is an approximate version of the equation for the functions  $\Phi_{kn}(r, \omega)$ , which diagonalize the Green's function in GWA at arbitrary energy  $\omega$ ,  $\langle \Phi_{kn}(\omega) | G^{-1}(\omega) | \Phi_{k'n'}(\omega) \rangle = \delta_{kk'} \delta_{nn'} (\omega - \Delta_{kn}(\omega))$ , *i.e.*, it contains energy-dependent self-energy  $\Sigma'(r, r_1, \omega)$  and  $\Phi_{kn}(r_1, \omega)$ ; the eigenvalues, which are poles of the Green's function, are obtained from the equation  $E_{kn} = Re\Delta_{kn}(E_{kn})$ . At last, both equations are highly non-linear and uniqueness theorem does not exist for them. Particularly, the problem of choice of the physical solution from multiple solutions generated by GWA is discussed in ref.<sup>31</sup>. Thus, at the moment we are at the stage when even the form of the exchange-correlation potential for a self-energy in GW approximation is not derived and the question about relationship between Kohn-Sham and GWA energies remains open. It is interesting, however, that more accurate exchange-correlation functionals than the widely-used ones can be obtained for evaluation of the excitation energies: the authors of ref.<sup>5</sup> state that, on the one hand, a surprising degree of agreement between the exact ground-state Kohn-Sham eigenvalue differences and excitation energies, for excitations from the highest occupied orbital to the unoccupied orbitals has been achieved for small systems; on the other hand, that “*the popular LDA and GGA functionals are nowhere near sufficiently accurate*”<sup>5</sup>.

### B. Band structure and spectral weights.

The PES-based experiments provide also the information on the spectral-weights of QPs,  $Z_\varepsilon$ . As was discussed above, the “self-energy” in Kohn-Sham equation (1) does not depend on energy and, therefore, corresponding spectral weight, defined in the perturbation theory as  $\left( Z_{k\lambda} = [1 - \partial\Sigma(E)/\partial E]^{-1} \right)_{E=E_{k\lambda}}$ , is always equal to unity. Insufficiency of the DFT-based approach is seen also from the Slüter & Sham's equation for the exchange-correlation potential: since it is based on the equalities of model and genuine electron densities of many-electron system, which are integral characteristics, it does not provide the equation for spectral weights of

the excitations. Contrary to that the self-energy does depend on energy giving birth to the spectral weight of the GW-QPs  $Z_\varepsilon < 1$ ; the remaining part of the spectral weight is shifted to incoherent excitations. It is instructive to represent the spectral weight in terms of magnitudes, encoded in the VASP. Let us write the equations for the Green's functions, corresponding to Eqs.(1),(2):

$$G^{-1}(E) = G_{DFT}^{-1}(E) - (\Sigma'(E) - v_{xc}). \quad (3)$$

Within the “one-shot” ( $G_0W_0$ ) approximation  $E = \varepsilon_{kn}$  and we obtain

$$Z_{kn} \simeq \frac{E_{kn} - \varepsilon_{kn}}{Re\Sigma_{GW}(\varepsilon_{kn}) - \left( v_{xc}^{(GGA)} \right)_{kn}}. \quad (4)$$

This relation is fulfilled by the magnitudes  $E_{kn}, \varepsilon_{kn}, \left( v_{xc}^{(GGA)} \right)_{kn}, \Sigma_{GW}(\varepsilon_{kn})$ , which are generated by VASP. As seen from Eq.(4) in the form<sup>18</sup>,

$$E_{kn} = \varepsilon_{kn} + Z_{kn} \left[ Re\Sigma'_{GW}(\varepsilon_{kn}) - \left( v_{xc}^{(GGA)} \right)_{kn} \right], \quad (5)$$

the role of the coefficient in the first term of the quasiparticle-energy expansion with respect to presumably small perturbation  $Re\Sigma(\varepsilon_{kn}) - v_{xc}$ , is played by the spectral weight. If the perturbation theory works,  $E_{kn} - \varepsilon_{kn} < (v_{xc} - \Sigma)_{kn}$  everywhere. Our calculations confirm that this inequality is valid for iron silicides. A comparison of behavior of these two differences,  $k$ -dependence of the spectral weights and an analysis of contributions from different electrons into these  $k$ -dependences are given in Sec.(III C).

### III. IRON SILICIDES

The calculations presented in this paper are performed using the Vienna Ab initio Simulation Package (VASP)<sup>13</sup> with Projector Augmented Wave (PAW) pseudopotentials<sup>14</sup>. The valence electron configurations  $3d^6 4s^2$  are taken for *Fe* atoms and  $3s^2 3p^2$  for *Si* atoms. One part of calculations is based on the density functional theory where the exchange-correlation functional is chosen within the Perdew-Burke-Ernzerhoff (PBE) parametrization<sup>15</sup> and the generalized gradient approximation (GGA).

In the GW part of calculations implemented in VASP<sup>16</sup> we report only one-shot approximation, so-called  $G_0W_0$ . The GGA Kohn-Sham band structure and eigenfunctions were taken as the input for the GW calculations. The self-energy  $\Sigma$  is computed as  $\Sigma \approx iG^{GGA}W^{GGA}$ . Throughout both GGA and GWA calculations the plane wave cutoff energy is 500 eV, the Brillouin-zone integrations are performed on the grid Monkhorst-Pack<sup>17</sup> special points  $10 \times 10 \times 10$  for  $Fe_3Si$  and  $12 \times 12 \times 6$  for  $\alpha - FeSi_2$  and Gauss broadening with smearing 0.05eV is used. For all GW calculations the number of frequencies is 500 and 160 electronic bands are used. We use the complex shift of 0.043 eV for the calculation of self-energy.

### A. Iron Silicides structure

The calculations are performed for two iron silicides,  $Fe_3Si$  and  $\alpha - FeSi_2$ . The compound  $Fe_3Si$  belongs to  $DO_3$  structural type with the space symmetry group  $Fm\bar{3}m$ . The iron atoms have two nonequivalent crystallographic positions in  $fcc$  lattice, namely,  $Fe^{(1)}$  and  $Fe^{(2)}$  have different nearest surroundings:  $Fe^{(1)}$  has eight  $Fe^{(2)}$  nearest neighbors which form a cube, whereas the  $Fe^{(2)}$  is in the tetrahedral surrounding of both  $Si$  and  $Fe^{(1)}$  atoms.

The iron bi-silicides have several structural modifications. The most stable phases are  $\alpha - FeSi_2$  and  $\beta - FeSi_2$  phases<sup>23,24</sup>. The compound  $\alpha - FeSi_2$  has tetragonal lattice with  $P4/mmn$  space symmetry group with one molecule per unit cell. Each iron atom here is located in the center of cube, consisting of the silicon atoms. This structure contains the planes which are formed by only iron and by only silicon atoms. These planes are orthogonal to tetragonal axis. Two planes formed by silicon atoms are separated by wide empty cavity, which does not contain the iron atoms. According to our calculations this cavity is expected to play essential role in the transport properties of  $\alpha - FeSi_2$ .

The rhombohedral cell have been used for the  $Fe_3Si$  calculations. The equilibrium parameters and the distances between nearest  $Fe$  and  $Si$  atoms for the  $Fe_3Si$  and  $\alpha - FeSi_2$  structures have been found from the full optimization of the structure geometries within GGA and are shown in Tab. (I). The GW calculation have been performed with the same structural parameters.

Both spin-polarized GGA and GW result in metallic states, ferromagnetic for  $Fe_3Si$  and paramagnetic with zero-spin  $Fe$  atoms for  $\alpha - FeSi_2$ . For this reason all further calculations for  $\alpha - FeSi_2$  have been performed within non-spin-polarized version of VASP. The structural inequivalence of the  $Fe$ -atoms' surroundings in the  $Fe_3Si$  reflects itself in both magnetic moment values and

the contributions of  $Fe$ -ions'  $d$ -states into electron density of states. The magnetic moment  $M_{Fe1}$  of  $Fe^{(1)}$  atom is higher than the free-atom moment,  $M_{Fe1}^{GGA} = 2.52\mu_B$  and  $M_{Fe1}^{GWA} = 2.55\mu_B$  what corresponds approximately to the  $d^5$  configuration. The  $Fe^{(2)}$  atom has much lower

$Fe_3Si$	$\alpha - FeSi_2$
$a = 5.6\text{\AA} (5.65\text{\AA})$	$a = 2.70\text{\AA} (2.69\text{\AA})$
$R(Fe^{(1)} - Fe^{(2)}) = 2.45\text{\AA}$	$c = 5.13\text{\AA} (5.134\text{\AA})$
$R(Fe^{(2)} - Si) = 2.45\text{\AA}$	$z_{Si} = 0.272 (0.28)$
$R(Fe^{(1)} - Si) = 2.83\text{\AA}$	$R(Fe - Si) = 2.30\text{\AA}$
	$R(Si - Si) = 2.56\text{\AA}$

Table I: Relaxed lattice parameters and the equilibrium distances between nearest ions. The experimental values<sup>23</sup> are given in brackets.

moment,  $M_{Fe2}^{GGA} = 1.34\mu_B$  and  $M_{Fe2}^{GWA} = 1.40\mu_B$ . As will be seen from the analysis of DOS, the latter moments are formed by the delocalized  $d$ -states. The experimental values reported in works<sup>25</sup> and<sup>26</sup> are slightly different:  $M_{Fe2}^{exp} = 1.2\mu_B$ ,  $M_{Fe1}^{exp} = 2.4\mu_B$  in Ref.<sup>25</sup> and  $M_{Fe2}^{exp} = 1.35\mu_B$ ,  $M_{Fe1}^{exp} = 2.2\mu_B$  in Ref.<sup>26</sup>.

### B. Comparison of GGA and GW densities of electron states

Fig.(1) displays comparison of the GGA and GW densities of electron states (DOS) for  $Fe_3Si$  and  $\alpha - FeSi_2$ . The GGA part of results coincides with previous calculations of  $Fe_3Si$ <sup>25,27,28</sup> and  $\alpha - FeSi_2$ <sup>24,27,29</sup>. The general features of the DOS in both compounds and approximations are that the bands in the interval  $(-5, +5)$  eV around Fermi energy are formed by the  $d$ -electrons of iron with a slight admixture of  $s$ - and  $p$ -electrons of  $Si$  and  $Fe$ . The  $Si$  valent  $s$ - and  $p$ -electrons are delocalized in the wide energy region with smeared maximum around  $-4$  eV in both compounds. GWA changes the intensities of the peaks mainly in the energy region deeply under Fermi surface, but the changes in  $Fe_3Si$  and  $\alpha - FeSi_2$  are different. If in the GGA DOS of the  $Fe_3Si$  the peak located at  $E \sim -3.5$  eV is shifted by GWA for about 0.5 eV and made sharper, the GGA peaks in  $\alpha - FeSi_2$  DOS in approximately the same energy region (I, II in bottom panel of Fig.(1)) is washed out within the GW calculations. There is a difference in the GWA vs GGA changes in DOS for spin "up" (majority) and "down": while the GW spin-majority states remain almost untouched compared to GGA, the spin-minority GWA peaks are shifted towards the Fermi energy.

---

As was mentioned above, different chemical surroundings of the  $Fe$  atom positions, the cubic one for  $Fe^{(1)}$  by  $Fe^{(2)}$

---

atoms and the tetrahedral one for the  $Fe^{(2)}$  atoms by the

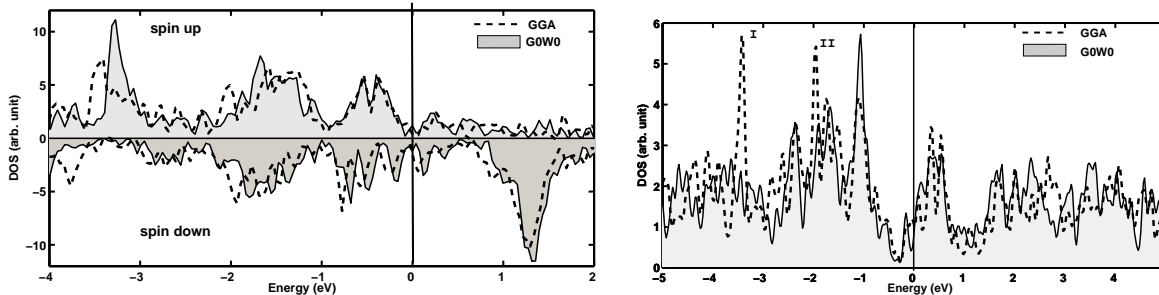


Figure 1: The left panel: The spin-polarised density of electron states for  $Fe_3Si$  in the interval of energies  $[-4\text{eV}, 2\text{eV}]$ . Since the GGA and the GW approximations produce different Fermi energies,  $\varepsilon_F^{GGA}(Fe_3Si) = 7.88\text{ eV}$  and  $\varepsilon_F^{GW}(Fe_3Si) = 8.44\text{ eV}$ , the plots are aligned for comparison by placing the zero in the energy axis of both plots at Fermi energy. The right panel: The DOS for  $\alpha-FeSi_2$  in the energy interval  $[-5,5]\text{eV}$  with the same type of alignment of the energy axes;  $\varepsilon_F^{GGA}(\alpha-FeSi_2) = 9.34\text{ eV}$  and  $\varepsilon_F^{GW}(\alpha-FeSi_2) = 10.03\text{ eV}$ .

$Fe^{(1)}$  and  $Si$  atoms as nearest neighbors reflect themselves in different behavior of partial  $d$ -electron DOS. It

is illustrated in Fig.(2).

The general shape of partial  $d$ -DOS is not changed by GWA. The  $d$ -states of  $E_g$  symmetry of  $Fe^{(1)}$  as well as  $Fe^{(2)}$  do not contribute into DOS at the Fermi level in both in LDA and GWA (panel (A), (C), Fig.(2)). As seen from Fig.(2), panels (A),(B), the contribution to the magnetic moment on  $Fe^{(1)}$  from  $E_g$  -orbitals (positive DOS in (A)) compensated by the contribution from  $T_{2g}$ -orbitals ( the negative middle peak in (B)). This means that the  $T_{2g}$ -orbitals are responsible for formation of the large quasi-localized magnetic moment at  $Fe^{(1)}$  atoms. It is also interesting that the usual splitting of the  $d$ -shell into  $T_{2g}$ - and  $E_g$ - symmetries is violated here by the contribution from exchange interaction: as seen from (A) and (B) panels the  $E_g$ -peak is in-between two  $T_{2g}$ -peaks. A different behavior is demonstrated by  $d$ -electrons of  $Fe^{(2)}$ : its  $d$ -DOS is spread in a wide region of energies. The  $d$ -electrons of both  $T_{2g}$ - and  $E_g$ - symmetries contribute to formation of magnetic moment of  $Fe^{(2)}$ . The delocalization of  $Fe^{(2)}$   $d$ -electrons reflects itself in the smaller moment than the one on  $Fe^{(1)}$ . The  $d$ -DOS of iron in  $\alpha-FeSi_2$ , where  $Fe$  atoms also have  $Si$  atoms as neighbors, displays behavior similar to  $Fe^{(2)}$  partial DOS for  $d$ -electrons in  $Fe_3Si$ . However only these delocalized electrons are not able to form magnetism in  $\alpha-FeSi_2$ . Indeed, the criterium for magnetism formation for the delocalized electrons is much harder to fulfil than for the case of localized electrons whose role is played by  $T_{2g}$ -electrons of  $Fe^{(1)}$  in  $Fe_3Si$ . The absence of magnetism in  $\alpha-FeSi_2$  is easy to understand on the basis of well-known Stoner's model for a magnetism of the delocalized electrons: the criterium  $Jg(\varepsilon_F) > 1$  is not fulfilled since the density of electron states  $g(\varepsilon_F)$  at the Fermi energy  $\varepsilon_F$  is too small (here  $J$  is exchange integral between delocalized electrons). An alternative mechanism of the mag-

netism supression would be a formation of the low-spin state within the localized  $d$ -electron picture. This state could be formed if the crystal-field splitting of the  $d$ -shell was stronger than the Hund-exchange one. However, the density of  $d$ -electron states does not contain bright peaks which might be interpreted as former  $d$ -levels splitted in the crystal field. Thus, one can conclude that if GGA and GWA are good approximations for  $\alpha-FeSi_2$ , the key mechanism of the magnetism destruction in this compound is the delocalization of  $d$ -electrons.

The most pronounced changes in GWA compared to GGA are experienced by  $T_{2g}$  electrons. It is illustrated on Fig.(2), panels (E,F) for  $\alpha-FeSi_2$ : two peaks (I and II) seen in the GGA DOS which have been mentioned above and washed out in the GWA are formed namely by  $T_{2g}$  electrons. The same is valid for the "down" spin  $T_{2g}$  states in the vicinity of the Fermi level in  $Fe_3Si$  (panel (D) in Fig.(2)). At the same time the well-expressed localized peaks formed by  $E_g$  orbitals remain intact. This is understandable: the GWA is the approximation which takes into account the effects of screening which is provided namely by the delocalized electrons. These effects are taken into account within the GGA and GWA differently and, therefore, one can expect that the difference will be more pronounced for these types of electrons.

### C. Comparison of GGA and GW band structures and analysis of the spectral weights

The Kohn-Sham band structure calculated within GGA does not differ from the known results for  $Fe_3Si$ <sup>25, 28</sup> and for  $\alpha-FeSi_2$ <sup>24, 29, 30</sup>. Here we compare the GGA and GW bands in some of symmet-

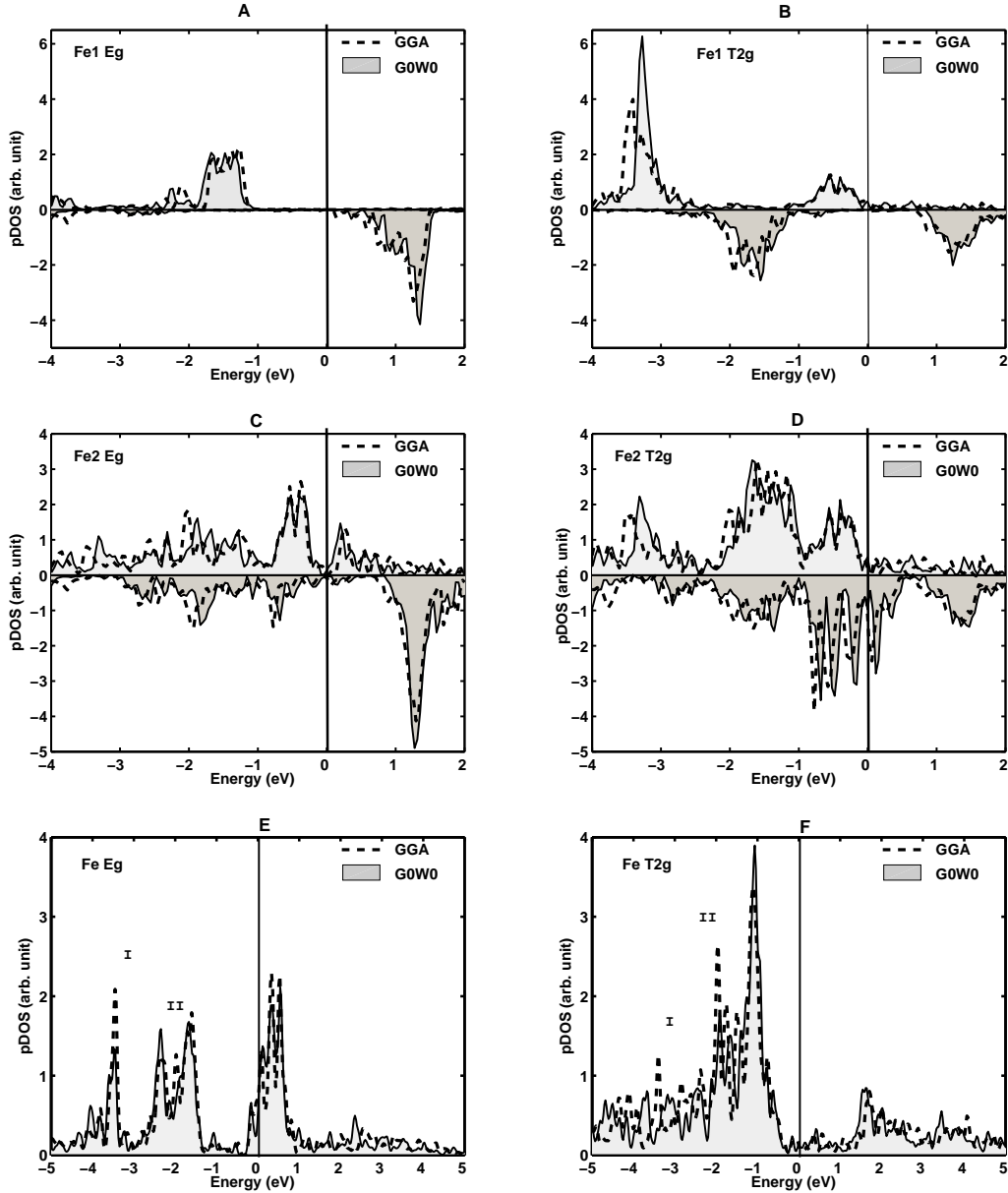


Figure 2: The partial spin-polarised  $d$ -electron DOS for  $Fe_3Si$  (upper four panels, (A),(B),(C),(D)) and  $\alpha - FeSi_2$  (lower two panels, (E),(F)). Left panels display the contribution to DOS from  $d_{z^2}$ - and  $d_{x^2-y^2}$ - states ( $E_g$ ), while the right ones show the contribution from  $d_{xy}$ - ,  $d_{xz}$ - and  $d_{yz}$ - states ( $T_{2g}$ ).

ric directions. Figs.(3) and (4) show the band structure for  $Fe_3Si$  in the directions  $\Gamma X$  and  $\Gamma L$ , and for  $\alpha - FeSi_2$  in the directions  $\Gamma X$ ,  $\Gamma M$  and  $\Gamma Z$ , where  $\Gamma = (0, 0, 0)$ ,  $X = (2\pi/a)(1, 0, 0)$ ,  $L = (\pi/a)(1, 1, 1)$ ,  $M = (2\pi/a)(1, 1, 0)$ ,  $Z = (2\pi/c)(0, 0, 1)$ .

We report here the results of the comparison only for the part of the GGA and GWA band structures which are within several electron-volts vicinity of the Fermi energies (remind that GGA and GWA generate different Fermi energies, see the capture to Fig.(1)). The bands are named in accordance with their symmetries in the  $\Gamma$ -point. The closest to the Fermi energy three filled spin-up bands for

the  $Fe_3Si$  in Fig.(3, left) near  $\Gamma$ -point, the doublet  $E_g$  and the triplet  $T_{2g}$ , are formed by the  $d$ -electrons of  $Fe$  atoms. First empty band ( $A_{1g}$ ) near  $\Gamma$ -point is formed by the  $s$ -states of both  $Fe$  and  $Si$  atoms.

The GGA and GWA band structures for  $\alpha - FeSi_2$  are shown in Fig.(4). Here the closest to the Fermi energy filled bands are formed by the  $d$ -orbitals of  $Fe$  atoms near  $\Gamma$ -point ( $D_{4h}$  group) are  $B_{1g}(d_{x^2-y^2})$ ,  $A_{1g}(d_{z^2})$ , the doublet  $E_g(d_{xz}, d_{yz})$  and  $B_{2g}(d_{xy})$ . The lowest shown band ( $A_{2u}$ ) is formed by the  $s$ -electrons of  $Fe$  and  $p$ -electrons of  $Si$ . Again we observe the same tendency: namely the delocalized states, in this case,  $s$ - and

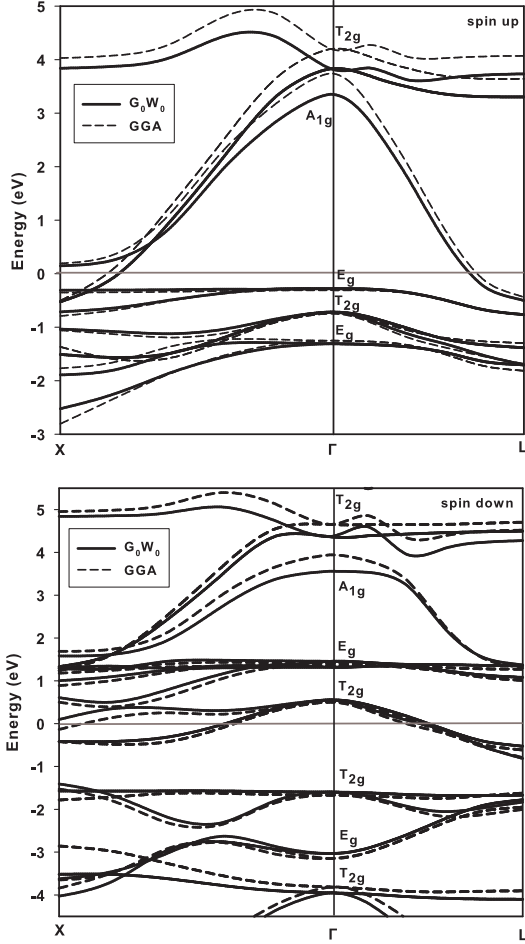


Figure 3: The GGA and GW spin-up (top) and spin-down (bottom) bands for  $Fe_3Si$ . Zero in the energy axis of GGA and GWA plots is chosen at corresponding Fermi energies.

$p$ -states, show the largest difference in GGA and GWA. If the band formed by  $d$ -electrons close to the Fermi energy remain almost untouched, the lowest  $sp$  band is shifted in GWA by  $\sim 1$  eV. First empty band ( $E_u$ ) near  $\Gamma$ -point is formed by the  $p$ -states of both  $Fe$  and  $Si$  atoms. In general the GGA *vs* GWA shift is around half of electron-volt for the excited states, while the band shape remains the same. As seen at the right panel of Fig.(4) in the  $\Gamma Z$  direction, the purely  $d$ -bands are completely flat, while the dispersion which arises near the boundaries is due to the admixture of  $s$  and  $p$  states. Analogous admixture of  $sp$  electrons is observed around the boundary points  $X$  and  $M$ . This is easy to understand since the motion along  $\Gamma X$  direction in the  $k$ -space corresponds to motion from the  $Fe$  atoms plane to the plane of  $Si$  atoms in real space;  $Si$  atoms do not have  $d$ -electrons and can admit the  $s$ - and  $p$ -states only.

Here we return to the question asked in Sec.(IIB), which electrons mainly are responsible for the deviations of GWA from GGA results. Let us consider the example of two  $E_g$  and  $T_{2g}$  filled bands of quasiparticles for spin

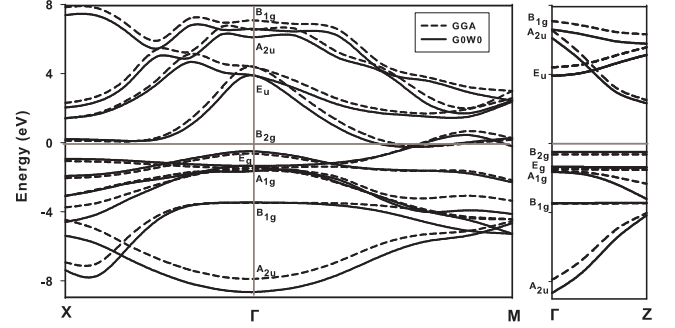


Figure 4: The band structure of  $\alpha - FeSi_2$ ; zero in the energy axis of GGA and GWA plots is chosen at corresponding Fermi energies.

“up” shown in Fig.(3).

First general feature seen from both Fig.(5) and Fig.(6) is that the spectral weights  $Z_{kn}$ , that within the Kohn-Sham approach are equal to one by construction, within the GWA are strongly decreased. Second feature, somewhat surprising, is that the non-monotonous behaviour of  $Z_{kn}$  arises everywhere where an admixture of delocalized electron states is present. Indeed, one observes that near the  $X$  point of the Brillouin band it is the admixture of  $s$ - and  $p$ -electrons to  $d$ -states for the band  $T_{2g}^{(1)}$  of  $Fe_3Si$  causes the changes in the  $Z_{kn}$ ; the difference  $Re\Sigma' - v_{xc}$  is changed faster than  $E_{kn} - \varepsilon_{kn}$  (see panel A at Fig.(5)). The picture for the empty bands is different: the  $s$ - and  $p$ -states of  $Si$  and  $d$ -states of  $Fe$  are mixed in the center of the band, whereas the contribution of the  $d$ -states is increased around boundary points  $X$  and  $L$ . The quasiparticle energies of the excited states are lower than their Kohn-Sham counterparts. Again, the largest difference is observed in the those parts of the energy spectrum where the contributions from  $s$ - and  $p$ -states becomes significant.

As seen from Fig.(6), the spectral weights  $Z_{kn}$  of the quasiparticles in  $\alpha - FeSi_2$  also show a strongly non-monotonous dependence on  $k$ . For example, the spectral weight  $Z_{k,B_{1g}}$  of the  $B_{1g}$  band in the direction  $\Gamma X$  (second from top panel in Fig.(6,B) shows sharp changes in the interval  $0.55 < Z_{k,B_{1g}} < 0.8$  due to much faster dependence on  $k$  of the difference  $(\Sigma' - v_{xc})$  than of the  $(E_{QP} - \varepsilon_{GGA})$  one. The lower part of the panel B in Fig.(6) explains the reason: again, the closer to the  $X$  point the higher contribution from the delocalized  $s$ -electrons. This confirms, thus, the general tendency noticed above.

#### IV. DISCUSSION AND CONCLUSIONS

The comparison of the band structures obtained in the *ab initio* calculations within the VASP for  $Fe_3Si$  and  $\alpha - FeSi_2$  in GGA and  $G_0W_0A$  shows that in gen-

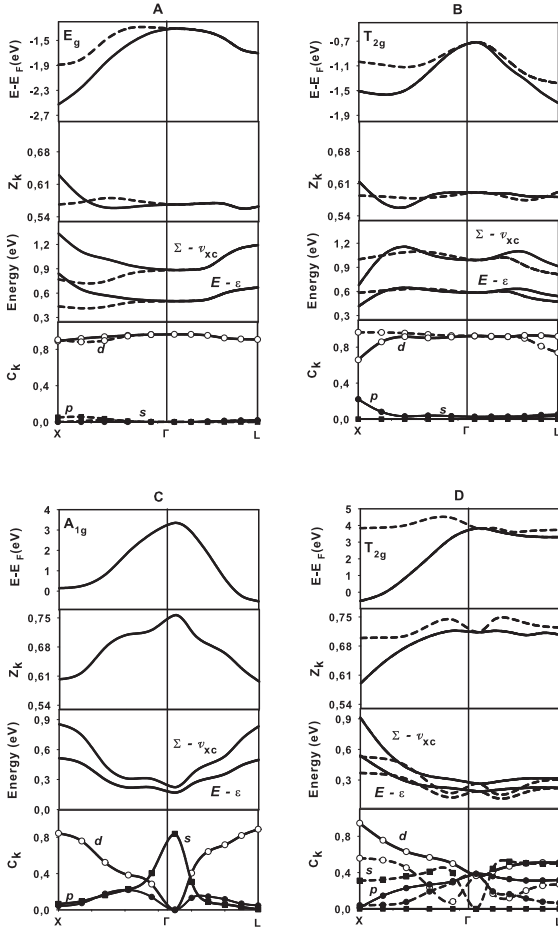


Figure 5:  $Fe_3Si$  quasiparticle filled bands (top panels), their spectral weights  $Z_k$  (second from the top), the  $k$ -dispersion of numerator and denominator of Eq.(4) (third from the top) and the character coefficients  $C_k$  (bottom panels, see text). The letters label different characters:  $d$  and  $p$  stand for the empty and filled circles correspondingly, the black squares denote  $s$  character. The filled bands are shown in (A) and (B) panels, while (C),(D) display the empty ones. The dashed and solid lines on (A) panel denote the non-degenerate bands  $E_g$ . The dashed and solid lines on (B), (D) panel denote non-degenerate and double degenerate bands  $T_{2g}$ .

eral the bands shape is similar. The difference between GGA and GWA bands becomes more pronounced in those parts of the Brillouin zone where the delocalized states give noticeable contribution into quasi-particle energies. This observation is somewhat unexpected since both approximations are designed for description of well delocalized (Fermi-liquid like) electrons. There are at least two sources which can contribute to this difference. First is the fact that the standard GGA is not free from the self-interaction while GWA takes into account Fermi statistics by construction. Second source is that GGA and GWA are quite different approximations, as was discussed in Introduction.

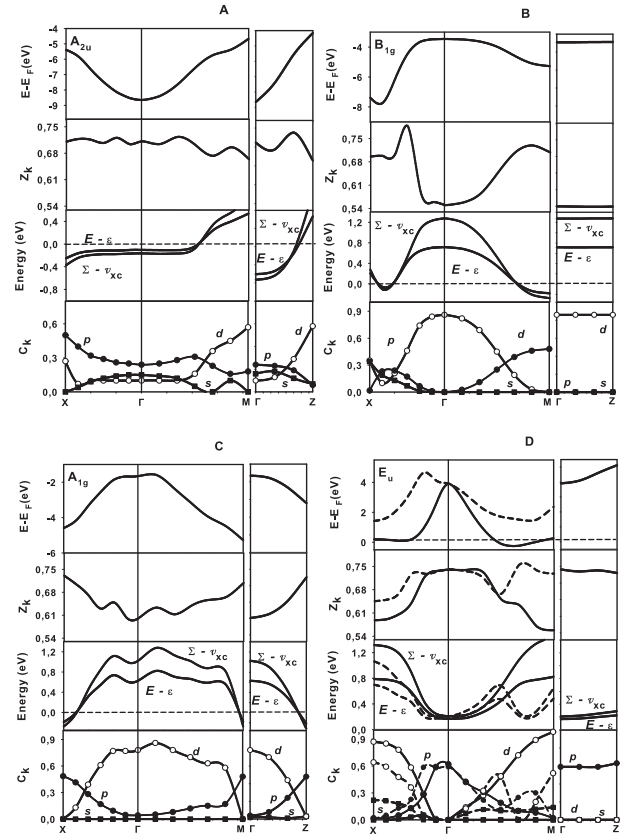


Figure 6: The  $\alpha - FeSi_2$  bands. The notations are the same as in Fig.(5), but the filled bands are imaged at the panels A,B,C, while the empty one is shown at D panel.

The other astonishing moment following from GWA calculations is that in spite of the fact that the electrons in both systems are well delocalized the spectral weights  $Z_{kn}$  of the quasiparticle bands  $E_{kn}$  are decreased almost by a half. One could assume that the reason for that is that the basis set is not sufficiently large, however, the results are not changed with further increase of number of bands which are taken into account. This means that the GWA indeed shifts the remaining part of the weight to the incoherent part of excitations.

Both GGA and GWA band structures and, correspondingly, the density of electron states, show that the  $d$ -electrons of those  $Fe$  atoms which have  $Si$  nearest neighbors, namely,  $Fe^{(2)}$  atoms for  $Fe_3Si$  and all  $Fe$  atoms in  $\alpha - FeSi_2$ , are more delocalized than the  $d$ -electrons of  $Fe^{(1)}$  atoms in  $Fe_3Si$  which have only the other  $Fe$  atoms as neighbors. The partial density of states of  $Fe^{(1)}$   $d$ -electrons with  $E_g$  and  $T_{2g}$  symmetry in the  $\Gamma$  point has well-expressed peaks, the positions of which could be ascribed to a splitting in the crystal field. However, this splitting does not correspond to the standard picture of the quasiatomic levels  $\varepsilon_{T_{2g},\sigma}^0 d_{t\sigma}^\dagger d_{t\sigma} + \varepsilon_{E_g,\sigma}^0 d_{e\sigma}^\dagger d_{e\sigma}$ , from which the bands are formed, the interactions renormalize these “levels”

$\varepsilon_{T_{2g},\sigma}^0 \rightarrow \varepsilon_{T_{2g},\sigma}$  in such a way that their sequence becomes  $\varepsilon_{T_{2g},\uparrow} < \varepsilon_{T_{2g},\downarrow}, \varepsilon_{E_g,\uparrow} < \varepsilon_{T_{2g},\uparrow}$ .

We performed the calculations within the one-shot GW approximation ( $G_0W_0$ ), and it is worth to notice why this approximation is preferable compared to the fully self-consistent GWA. First, it often gives the results which describe PES experiments better (see, *e.g.*, refs.<sup>32,33,34</sup>). Second argument is connected with the nature of the self-consistency. Each term in the self-consistent perturbation theory (scPT) corresponds to whole series in the non-scPT. If we consider these corrections, we find that a part of corrections in each order of the non-scPT changes the matrix elements of the Coulomb interaction, actually, via corrections to the wave functions. The self-consistency loop changes the eigenfunctions which diagonalize the GW equation for the Green's functions, and, correspondingly, dresses the matrix elements of Coulomb interaction by the RPA (random phase approximation) graphs only. All other contributions to the wave functions, which arise in the same orders of non-scPT, and, correspondingly, to the matrix elements of Coulomb interaction, are not taken into account. However, in the case of non-homogeneous electron gas in real-material, where the gellium-like parts can coexist with strongly correlated liquid, the situation is not always obvious. The question how and to which

terms the vertex corrections should be applied remains highly non-trivial. This has been demonstrated, *e.g.*, in ref.<sup>35</sup>, where it was shown that the vertex corrections into effective interaction  $W$  may improve the results while turning on the corrections in the self-energy may lead to unphysical quasiparticle dispersion. At last, the calculations within GWA with the vertex corrections demand for much stronger computer resources than even scGWA. The ARPES experiments on iron silicides would be of great help in further understanding of these compounds and, possibly, could motivate more advanced theoretical approach to the problem.

### Acknowledgement

The authors thank for support from RFBR No. 14002-00186, the President of Russian Federation Grants (NSH-2886.2014.2 and NSH-924.2014.2) and Physics Department of RAS program "Electron correlations in systems with strong interaction". The calculations were performed with the computer resources of NRC "Kurchatov Institute" (ui2.computing.kiae.ru). I.S. thanks A.Ruban for useful discussion.

---

\* Electronic address: sandalov@kth.se; Corresponding author

- <sup>1</sup> S. A. Wolf, D. D. Awschalom, R. A. Buhrman, J. M. Daughton, S. von Molnar, M. L. Roukes, A. Y. Chtchelkanova and D. M. Treger, *Science* 294, 1488 (2001)
- <sup>2</sup> K. Ueda, Y. Kishi, Y. Ando, T. Sadoh and M. Miyau, *Appl. Phys. Lett.* 93, 132117 (2008)
- <sup>3</sup> R. Nakane, M. Tanaka and S. Sugahara, *Appl. Phys. Lett.* 89, 192503 (2006)
- <sup>4</sup> I. A. Yakovlev, S. N. Varnakov, B. A. Belyaev, S. N. Zharkov, M. S. Molokeev, I. A. Tarasov and S. G. Ovchinnikov, *JETP Lett.* 99, 527 (2014)
- <sup>5</sup> C. J. Umrigar, A. Savin, and Xavier Gonze in *Electronic Density Functional Theory: Recent Progress and New Directions*, edited by J. F. Dobson, G. Vignale and M. P. Das, (Plenum, N.Y., 1997) Are unoccupied Kohn-Sham eigenvalues related to excitation energies? p.1-10
- <sup>6</sup> E. Wimmer, H. Krakauer, M. Weinert, and A. J. Freeman, *Phys. Rev. B* 24, 864 (1981)
- <sup>7</sup> J. Kudrnovsky, N. Christensen and O. K. Andersen, *Phys. Rev. B* 43, 5924 (1991)
- <sup>8</sup> H. Jansen and A. J. Freeman, *Phys. Rev. B* 30, 561 (1984)
- <sup>9</sup> H. L. Skriver, *The LMTO method* (Springer, New-York, 1984)
- <sup>10</sup> O. K. Andersen, *Phys. Rev. B* 12, 3060 (1975)
- <sup>11</sup> H. Ueba, B. Gumhalter, *Progr. Surf. Sci.* 82, 193-223 (2007);
- <sup>12</sup> F. Aryasitiawan, O. Gunnarsson, *Rep. Prog. Phys.* 61, 237 (1998); W.G. Aulbur, L. Jönsson, J.W. Wilkins, Quasiparticle calculations in solids. *Solid State Phys.* 54, 1-218 (2000).

- <sup>13</sup> G. Kresse and J. Furthmüller. *Comput. Mat. Sci.* 6, 15 (1996); G. Kresse and J. Furthmüller. *Phys. Rev. B* 54, 11169 (1996)
- <sup>14</sup> P. E. Blöchl, *Phys. Rev. B* 50, 17953 (1994); G. Kresse and J. Joubert, *Phys. Rev. B* 59, 1758 (1999)
- <sup>15</sup> J. P. Perdew, K. Burke, and M. Ernzerhof. *Phys. Rev. Lett.* 77, 3865 (1996); P. Perdew, K. Burke, and M. Ernzerhof. *Phys. Rev. Lett.* 78, 1396 (1997)
- <sup>16</sup> M. Shishkin and G. Kresse, *Phys. Rev. B* 74, 035101 (2006); F. Fuchs, J. Furthmüller, F. Bechstedt, M. Shishkin, and G. Kresse, *Phys. Rev. B* 76, 115109 (2007)
- <sup>17</sup> H. J. Monkhorst and J. D. Pack, *Phys. Rev. B* 13, 5188 (1976)
- <sup>18</sup> Giovanni Onida, Lucia Reining, Angel Rubio, *Rev. Mod. Phys.*, 74, pp.APRIL 2002;
- <sup>19</sup> John M. Wills, Mebarek Alouani, Per Andersson, Anna Delin, Olle Eriksson, Oleksiy Grechnev, Full-Potential Electronic Structure Method Energy and Force Calculations with Density Functional and Dynamical Mean Field Theory, p.151, the book 167 in *Springer Series in solid-state sciences Series*, Editors: M. Cardona, P. Fulde, K. von Klitzing, R. Merlin, H.-J. Queisser, H. Störmer.
- <sup>20</sup> T. Koopmans, *Physica* 1 (1-6), 104 (1934)
- <sup>21</sup> J. P. Perdew, R. G. Parr, M. Levy and J. L. Balduz, *Phys. Rev. Lett.* 49, 1691 (1982); M. Levy, J. P. Perdew and V. Sahni *Phys. Rev. B* 30, 2745 (1984); U. von Barth in *Electronic Structure of Complex Systems*, edited by P. Phariseau and W. M. Temmerman, NATO, ASI Series B, vol. 113 (1984).
- <sup>22</sup> L. J. Sham and M. Shlüter, *Phys. Rev. Lett.* 51, 1888 (1983); L. J. Sham and M. Shlüter, *Phys. Rev. B* 32, 3883

- (1985)
- <sup>23</sup> P. Villars and L. D. Calvert, Pearson's Handbook of Crystallographic Data for Intermetallic Phases (American Society for Metals, Materials Park, OH, 1985)
- <sup>24</sup> S. Eisebitt, J.-E. Rubensson, M. Nicodemus, T. Boske, S. Blugel, W. Eberhardt, K. Radermacher, S. Mantl and G. Bihlmayer Phys. Rev. B 50, 18330 (1994)
- <sup>25</sup> N. E. Christensen, J. Kudrnovský, C. O. Rodriguez, Int. J. Mater. Sci. Simu. 1, 1 (2007)
- <sup>26</sup> W. A. Hines, A. H. Menotti, J. I. Budnick, T. J. Burch, T. Litrenta, V. Niculescu and K. Raj, Phys. Rev. B 13, 4060 (1976)
- <sup>27</sup> E. G. Moroni, W. Wolf, J. Hafner, and R. Podloucky. Phys. Rev. B 59, 12860 (1999)
- <sup>28</sup> E. J. D. Carba and R. L. Jacobs, J. Phys. F: Met.Phys. 16, 1485 (1986)
- <sup>29</sup> R. Girlanda, E. Piparo, and A. Balzarotti. Journal of Applied Physics 76, 2837 (1994)
- <sup>30</sup> J. van Ek, P. E. A. Turchi, and P. A. Sterne, Phys. Rev. B 54, 7897 (1996)
- <sup>31</sup> F. Tandetzky, J. K. Dewhurst, S. Sharma and E. K. U. Gross, arXiv: 1205.4274v1 [cond-mat.str-el] 18 May 2012.
- <sup>32</sup> Noa Marom, Fabio Caruso, Xinguo Ren, Oliver Hofmann, Thomas Krzdrfer, James R. Chelikowsky, Angel Rubio, Matthias Scheffler, and Patrick Rinke, arXiv: 1216.0416 [cond-mat.mtrl-sci] 2 Nov 2012, Phys. Rev. B 86, 245127 (2012).
- <sup>33</sup> Adrian Stan, Nils Erik Dahlen, and Robert van Leeuwen, arXiv: 1205.4274v1 [cond-mat.other] 09 July 2009.
- <sup>34</sup> C. Rostgaard, K. W. Jacobsen, and K. S. Thygesen arXiv: 1001.1274v1 [cond-mat.mtrl-sci] 8 Jan 2010, Phys. Rev. B 81, 085103.
- <sup>35</sup> Andrew J. Morris, Martin Stankovski, Kris T. Delaney, Patrick Rinke, P. Garca-Gonzlez, and R. W. Godby, Phys. Rev. B 76, 155106.